Interpreting the Catalytic Voltammetry of an Adsorbed Enzyme by Considering Substrate Mass Transfer, Enzyme Turnover, and Interfacial Electron Transport

Torsten Reda and Judy Hirst*

Medical Research Council Dunn Human Nutrition Unit, Wellcome Trust/MRC Building, Hills Road, Cambridge, CB2 2XY, U. K.

Received: August 24, 2005; In Final Form: October 24, 2005

Redox active enzymes can be adsorbed onto electrode surfaces to catalyze the interconversion of oxidized and reduced substrates in solution, driven by the supply or removal of electrons by the electrode. The catalytic current is directly proportional to the rate of enzyme turnover, and its dependence on the electrode potential can be exploited to define both the kinetics and thermodynamics of the enzyme's catalytic cycle. However, observed electrocatalytic voltammograms are often complex because the identity of the rate limiting step changes with the electrode potential and under different experimental conditions. Consequently, extracting mechanistic information requires that accurate models be constructed to deconvolute and analyze the observed behavior. Here, a basic model for catalysis by an adsorbed enzyme is described. It incorporates substrate mass transport, enzyme kinetics, and interfacial electron transport, and it accurately reproduces experimentally recorded voltammograms from the oxidation of NADH by subcomplex Iλ (the hydrophilic subcomplex of NADH:ubiquinone oxidoreductase), under a range of conditions. Mass transport is imposed by a rotating disk electrode and described by the Levich equation. Interfacial electron transport is controlled by the electrode potential and characterized by a dispersion of rate constants, according to the model of Léger and co-workers.[33] Here, the Michaelis−Menten equation is used for the enzyme kinetics, but our methodology can also be readily applied to derive and apply analogous equations relating to alternative enzyme mechanisms. Therefore, our results are highly relevant to the interpretation of electrocatalytic voltammograms for adsorbed enzymes in general.

Introduction

In protein-film voltammetry (PFV) redox-active enzyme or protein molecules are adsorbed onto an electrode surface and interrogated by electrochemical techniques.[1−4] Typically, the electrode potential (the "driving force") is varied, and the rate of a redox reaction is monitored precisely via the current which flows between the enzyme or protein and the electrode. Therefore, a complete and integrated picture is obtained by quantifying both the thermodynamics and kinetics of the redox reaction. PFV owes its success to the immobilization of the protein or enzyme on the electrode surface, to remove kinetic limitations imposed by its slow diffusion from the bulk solution, and an ever increasing number of studies have focused on this experimental design. For example, extensive studies have characterized the reactions and interconversions of iron−sulfur clusters in ferredoxins by applying models which incorporate both thermodynamics and kinetics to interpret the voltammetric results (see, for example, refs 5−9). PFV is also being exploited to study the mechanisms of catalysis by complex redox enzymes (see, for example, refs 10−15), though two major challenges are inherent to this approach. The first challenge is to devise a method of "coupling" the enzyme to the electrode, so that interfacial (long-range) electron transfer does not control the rate of enzyme turnover. The second is to apply a realistic model to accurately interpret the observed voltammetry, to provide thermodynamic and kinetic information pertaining to the interconversion of catalytic intermediates which may not be readily accessible by conventional techniques.

For a complex enzyme adsorbed on an electrode surface, three processes may contribute to determining the rate of electrocatalysis:[16,17] the supply of the substrate from bulk solution, the intrinsic kinetic properties of the enzyme (e.g., substrate binding and conversion, intramolecular electron transport), and the supply or removal of electrons by the electrode (Scheme 1A). If the substrate supply is rate limiting (substrate is depleted at the electrode surface) then the rate of catalysis is mass transport limited, and the enzyme's characteristics are obscured. Consequently, a rotating disk electrode is typically used to control mass transport to the surface, because high rates of supply can be achieved, and because the system can be modeled mathematically and described by a simple equation, the Levich equation.[18,19] The characteristics of the enzyme are also obscured if electrical contact with the electrode is poor, so that, even at high over-potential, the rate of enzyme turnover is dominated by interfacial electron-transfer limitations. The rate of interfacial electron transfer, at a given overpotential, is affected by a number of factors including the Marcus reorganization energy, the distance between enzyme cofactor and electrode surface, and the nature of the intervening medium.[20−22] Consequently, optimization of the interface is a requirement for the success of an experiment, and significant effort has been made to create "designer" interfaces which provide homogeneous, stable monolayers, and which may be amenable to spectroscopic techniques (see, for example, refs 1, 23−27). An alternative approach, which has proved highly successful, is to adsorb the enzyme

* Corresponding author. Phone: +44 1223 252810. Fax: +44 1223 252815. E-mail: jh@mrc-dunn.cam.ac.uk.

10.1021/jp054783s CCC: $33.50
Published on Web 01/05/2006

SCHEME 1: Mechanistic Schemes for Catalysis by Subcomplex Iλ Adsorbed on an Electrode Surface[a]

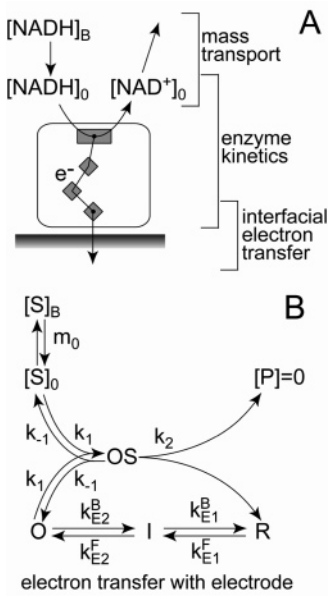

[a] (A) Three processes may control the catalytic rate: (i) mass transport of NADH from bulk solution ($[NADH]_B$) to the electrode surface ($[NADH]_0$) and of NAD^+ away from the surface; (ii) the enzyme kinetics, comprising substrate binding and product release, the catalytic interconversion, and electron transport through the enzyme via the iron−sulfur clusters; (iii) interfacial electron transfer between the electrode and the receiver/donor cofactor in the enzyme. (B) Generic mechanism for the two electron oxidation of a substrate by an enzyme adsorbed on an electrode surface, assuming that intramolecular electron transfer is not rate limiting. The oxidized form of the enzyme (O) converts substrate to product according to the Michaelis−Menten equation (described by k_1 (M^{-1} s^{-1}), k_{-1} (s^{-1}) and k_2 (s^{-1})); the substrate concentration at the enzyme ($[S]_0$) is maintained by mass transport from bulk solution ($[S]_B$) and product is removed. Following reaction, the reduced enzyme (R) is reoxidized by two, one electron transfer steps (described by the two potentials E_1 and E_2 (V) and the interfacial rate constants, $k^{F/B}_{Ei}$ (s^{-1})) via the singly reduced intermediate (I).

directly onto a freshly polished pyrolytic graphite edge (PGE) surface.[1−4] Most likely the rough, hydrophilic surface provides a wide range of microenvironments[28−32] facilitating adsorption of the native protein and direct contact with the electrode.

In an ideal situation interfacial electron transfer is fast enough that an equilibrium of the oxidized and reduced "contacting" cofactor is maintained at all electrode potentials. Consequently, as the potential is scanned the steady-state current becomes potential independent, and the limiting current is a result of either mass-transport or enzyme limitations. Using either the Butler−Volmer or Marcus equations for interfacial electron transfer, the Levich equation for mass transport, and the Michaelis−Menten equation for enzyme turnover, Heering and co-workers were able to formulate a mathematical model describing the catalytic voltammetry of an adsorbed enzyme under conditions in which a limiting current is readily attained (we refer to this as "Heering's Model" or "Model 1").[17] However, for the NiFe hydrogenase from *Allochromatium vinosum*, limiting currents could not be attained (within the experimental potential window) under conditions in which the turnover rate was high (for example, high temperature), suggesting that interfacial electron transport influences the rate of catalysis. Léger and co-workers proposed an elegant explanation for this behavior.[33] They suggested that a dispersion in the interfacial electron transfer rates exists, due to a distribution in the orientation of the adsorbed enzyme molecules and hence a distribution in the distance over which electron transfer must occur. Consequently, using a simple scheme which included interfacial electron transfer and a first-order reaction for the substrate conversion, they were able to successfully model the observed voltammetry of the NiFe hydrogenase under these conditions (we refer to this as "Léger's Model" or "Model 2").[33]

In this paper, we describe and interpret the electrocatalytic two-electron oxidation of NADH by the Iλ subcomplex of NADH:ubiquinone oxidoreductase (complex I) from bovine heart mitochondria. Complex I is a highly complicated redox enzyme. It catalyses the oxidation of NADH and the reduction of ubiquinone, and uses the available redox energy to pump four protons (per two electrons transferred) across the inner mitochondrial membrane.[34,35] The mechanism of energy transduction is not known. Subcomplex Iλ comprises the hydrophilic, membrane-extrinsic arm of complex I.[36,37] It contains 14 or 15 subunits, a flavin mononucleotide cofactor (FMN) which is the direct oxidant of NADH, and eight iron−sulfur clusters which form a chain through the enzyme.[38,39] In complex I the iron−sulfur clusters form a connection between the FMN and bound ubiquinone; in our experiment they probably form a connection to the electrode instead (see Scheme 1A).

Previously, subcomplex Iλ was demonstrated to catalyze the reversible interconversion of NADH and NAD^+, when adsorbed on a PGE electrode.[40] Here, we investigate, in detail, NADH oxidation by subcomplex Iλ, and we formulate a mechanistic model to quantify and explain the observed voltammetric behavior. Under conditions in which both mass transport and substrate concentration are high, the voltammograms closely resemble those exhibited by *A. vinosum* NiFe hydrogenase,[33] suggesting that interfacial electron transfer is governed by a distribution in the rate constants. However, at lower substrate concentrations and/or lower mass transport rates the voltammograms change in shape, providing insights into substrate/enzyme interactions, such as substrate binding constants. Under these conditions (when the surface concentration of the substrate is not equal to the bulk concentration at all potentials) Léger's simple reaction scheme does not apply. Importantly, the mass-transport and substrate concentration independent limit may not be attainable for all adsorbed enzymes: the substrate for NiFe hydrogenase (H_2) has an atypically high diffusion coefficient, and it binds strongly to the enzyme (K_m is low),[41] but neither of these characteristics apply to the enzyme described here. Consequently, we have developed a model which includes mass transport of substrate to the electrode surface, enzyme turnover according to the Michaelis−Menten equation, and interfacial electron transfer according to a distribution in electron transfer rate. Our model accurately reproduces the voltammetric characteristics of NADH oxidation by the Iλ subcomplex of NADH: ubiquinone oxidoreductase.

Experimental Procedures

Preparation of Subcomplex Iλ. Subcomplex Iλ was prepared from complex I (isolated from bovine heart mitochondria) as described previously,[36] except that 0.5% dodecyl-trimethylammonium bromide (DTAB, Sigma-Aldrich) was added to the protein solution before application to the sucrose gradient, and to the sucrose gradient. The final step, size exclusion chromatography, was carried out in the absence of detergent. Following purification, the subcomplex was concentrated to 10 mg ml^{-1} and stored as aliquots in liquid nitrogen.

Electrochemical Methods. A rotating disk PGE working electrode (geometric area 0.0314 cm^2, controlled by an EG&G

636 motor) was used in conjunction with a saturated calomel reference electrode (SCE) and a platinum counter electrode. The three compartment glass cell was thermostated using a water circulator. The central working electrode compartment contained 10 mM KCl (as supporting electrolyte) and 10 mM of each of the following buffers: potassium acetate, 2-morpholinoethane sulfonic acid (MES), N-cyclohexyl-2-aminoethane sulfonic acid (HEPES), and N-tris(hydroxymethyl)methyl-3-aminopropane sulfonic acid (TAPS). The reference electrode was separated by a Luggin sidearm, and the counter electrode was behind a Vycor glass frit to prevent contamination; these two compartments contained 0.1 M KCl as supporting electrolyte. NADH (Sigma) was repurified anaerobically immediately before use to remove NAD^+ [42] and added to the electrochemical cell from a 20 mM stock solution in Milli-Q water. All experiments were carried out in an anaerobic N_2 glovebox (Belle Technology, U. K., O_2 < 5 ppm), and were performed using an Autolab electrochemical analyzer PGSTAT30 (Eco Chemie, The Netherlands). The scan rate was typically 25 mV s^{-1} because, within the limits of enzyme stability, decreasing the scan rate did not affect the results, demonstrating that the voltammetry can be considered to be at steady state. Potentials are quoted relative to the standard hydrogen electrode (SHE, $E_{SHE} = E_{SCE} + 0.241$ V at 25 °C,[19] the SCE remained at room temperature).

Didodecyl-dimethylammonium bromide (DDAB, Sigma) micelles were prepared by dissolving DDAB in chloroform, evaporating the chloroform under a stream of nitrogen, and resolubilizing the DDAB to 1 mM in HPLC grade water (Sigma). Then, the DDAB solution was sonicated for 1 min. at 10 W using a 3.2 mm diameter microtip horn on a Misonix 3000 ultrasonic device (Misonix, NY). An aliquot of subcomplex Iλ was thawed, mixed (1:1) with 2 mM tris(2-carboxyethyl)phosphine hydrochloride (TCEP, Sigma) in Milli-Q water, and incubated for 1 h at room temperature. A PGE electrode was polished, using an aqueous 1 μm alumina suspension and napped cloth (Buehler, IL), then sonicated for 30 s in Milli-Q water, and dried. 0.5 μL of the DDAB solution was applied to the surface, then 0.5 μL of the Iλ solution was added, and mixed with the DDAB film.[43,44] The electrode was placed immediately into the electrochemical cell, and poised at the starting potential for 5 s before scanning.

Data Processing. Reference scans were recorded in the absence of NADH, or in the absence of subcomplex Iλ, to allow evaluation of changes in apparent electrode surface capacitance with potential, and detection of any background currents which may arise.[45,46] PGE electrodes are known to have a complex surface chemistry which may appear as a capacitative current.[29−32,47] The forward and backward scans were averaged for each cyclic measurement, then the reference scan was subtracted from the data. All data presented is from the second cycle in the measurement, because the first cycle often exhibits atypical capacitative currents, and because subsequent scans are identical to the second scan, except that they may differ in the magnitude of the catalytic current (<1% per scan).

Mathematical Formulation

A simple scheme for the two-electron oxidation of a substrate by an enzyme adsorbed on an electrode surface is presented in Scheme 1B. The enzyme's catalytic cofactor, in this case the FMN cofactor of complex I, can exist in three oxidation states: fully oxidized (O), semi-reduced (I), and fully reduced (R). Scheme 1B assumes that NADH only binds to the enzyme when the FMN is fully oxidized,[48] and that catalysis proceeds according to the Michaelis−Menten equation: reversible binding of the substrate to the active site is described by K_m (μM), and the reaction of the substrate-enzyme complex is irreversible and described by k_2 (s^{-1}).[49] The irreversible reaction comprises the catalytic transformation and any following steps, such as product dissociation, but it does not include regeneration of the active site. In our model, the reverse reaction (product re-binding and reduction) is prevented by constant dissipation of the product into the bulk solution. Following the catalytic transformation, the fully reduced cofactor is reoxidized by the electrode in two one electron steps, described by the potentials E_1 and E_2 (V) and the interfacial electron-transfer rate constant (see below), before substrate binds again. Experimentally, substrate is supplied to the electrode surface by mass transport at a controlled and known rate, imposed by rotation of the electrode.[18,19]

The first stage in deriving our model follows the procedure of Heering and co-workers,[17] who used the same reaction scheme (but in the reductive direction). The steady-state differential equations for the surface concentrations of the four enzyme intermediates (Γ_x, mol cm^{-2}) are the following:

$$\frac{d\Gamma_R}{dt} = 0 = -k^F_{E1}\Gamma_R + k^B_{E1}\Gamma_I + k_2\Gamma_{OS} \quad (1a)$$

$$\frac{d\Gamma_I}{dt} = 0 = k^F_{E1}\Gamma_R - k^B_{E1}\Gamma_I - k^F_{E2}\Gamma_I + k^B_{E2}\Gamma_O \quad (1b)$$

$$\frac{d\Gamma_O}{dt} = 0 = k^F_{E2}\Gamma_I - k^B_{E2}\Gamma_O - k_1S_0\Gamma_O + k_{-1}\Gamma_{OS} \quad (1c)$$

$$\frac{d\Gamma_{OS}}{dt} = 0 = k_1S_0\Gamma_O - k_{-1}\Gamma_{OS} - k_2\Gamma_{OS} \quad (1d)$$

S_0 is the substrate concentration at the surface (mol cm^{-3}). Γ_{Total} is the sum of all the different states:

$$\Gamma_{Total} = \Gamma_R + \Gamma_I + \Gamma_O + \Gamma_{OS} \quad (2a)$$

$$\Gamma_{Total} = \Gamma_{OS}\left(1 + \frac{\Gamma_O}{\Gamma_{OS}}\left(1 + \frac{\Gamma_I}{\Gamma_O}\left(1 + \frac{\Gamma_R}{\Gamma_I}\right)\right)\right) \quad (2b)$$

defining the Michaelis−Menten constant, K_m,

$$K_m = \frac{k_{-1} + k_2}{k_1} \quad (3)$$

and using expressions for the interfacial electron-transfer rate constants given by the Butler−Volmer equation[19] (k^F_{Ei} in the oxidative direction, k^B_{Ei} in the reductive direction, assuming symmetrical energy barriers and the same k_0 value for each step),

$$k^F_{Ei} = k_0\exp\left[\frac{0.5F}{RT}(E - E_i)\right] \quad (4a)$$

$$k^B_{Ei} = k_0\exp\left[\frac{-0.5F}{RT}(E - E_i)\right] \quad (4b)$$

$$\in_i = \frac{k^B_{Ei}}{k^F_{Ei}} = \exp\left[\frac{-F}{RT}(E - E_i)\right] \quad (4c)$$

the ratios in eq 2b can be rewritten as follows:

$$\frac{\Gamma_O}{\Gamma_{OS}} = \frac{K_m}{S_0} \tag{5a}$$

$$\frac{\Gamma_I}{\Gamma_O} = \epsilon_2 + \frac{S_0}{K_m}\frac{k_2}{k_{E2}^F} \tag{5b}$$

$$\frac{\Gamma_R}{\Gamma_I} = \epsilon_1 + \frac{k_2 S_0}{K_m k_{E1}^F}\left(\frac{\Gamma_O}{\Gamma_I}\right) \tag{5c}$$

Thus, the rate of enzyme turnover, V (s^{-1}) eq 6a, is given by eq 6b:

$$V = k_2\Gamma_{OS} \tag{6a}$$

$$V = \frac{k_2\Gamma_{Total}}{1 + \frac{K_m}{S_0}a + \frac{k_2}{k_0}b} \tag{6b}$$

$$a = 1 + \epsilon_2 + \epsilon_1\epsilon_2 \tag{6c}$$

$$b = \sqrt{\epsilon_1} + \sqrt{\epsilon_2}(1 + \epsilon_1) \tag{6d}$$

Heering's equation is derived directly from eq 6b, by equating enzyme turnover to mass transport.[17] Instead, we consider here dispersion in the interfacial electron-transfer rates, as proposed by Léger and co-workers.[33] The enzyme molecules are considered to be adsorbed on the surface in a random orientation, or in motion, such that electron transfer can occur from a variety of distances from the surface, with the smallest and largest distances separated by d_0 (Å). This produces a dispersion in k_0, where k_0^{max} refers to the maximum rate (which occurs at the smallest distance). Following Léger's methodology, the probability of an electron-transfer event with a given value of k_0 is $p(k_0)$,

$$p(k_0) = \begin{cases} (\beta d_0)^{-1}k_0^{-1} & \text{for } k_0^{min} < k_0 < k_0^{max} \\ 0 & \text{for any other value} \end{cases} \tag{7a}$$

$$k_0^{min} = k_0^{max}\exp(-\beta d_0) \tag{7b}$$

where β is the electron-transfer decay constant (Å^{-1}). β and d_0 are always a product, and so are considered together as βd_0. Thus, the overall rate of catalysis by the adsorbed enzyme, V (s^{-1}), is

$$V = \int_{k_0^{min}}^{k_0^{max}} V(k_0)p(k_0)dk_0 \tag{8a}$$

$$V = \int_{k_0^{max}}^{k_0^{max}} \frac{k_2\Gamma_{Total}}{1 + \frac{K_m}{S_0}a + \frac{k_2}{k_0}b} \cdot \frac{1}{\beta d_0 k_0}dk_0 \tag{8b}$$

$$V = \frac{k_2\Gamma_{Total}}{\beta d_0\left(1 + \frac{K_m}{S_0}a\right)}\ln\left[\frac{\left(1 + \frac{K_m}{S_0}a\right)k_0^{max} + k_2 b}{\left(1 + \frac{K_m}{S_0}a\right)k_0^{min} + k_2 b}\right] \tag{8c}$$

Finally, at steady-state the rate of enzyme turnover must equal the rate of substrate supply by mass transport:

$$m_0(S_B - S_0) = \frac{k_2\Gamma_{Total}}{\beta d_0\left(1 + \frac{K_m}{S_0}a\right)}\ln\left[\frac{\left(1 + \frac{K_m}{S_0}a\right)k_0^{max} + k_2 b}{\left(1 + \frac{K_m}{S_0}a\right)k_0^{min} + k_2 b}\right] \tag{9a}$$

Equation 9a can be applied to any form of mass transport for which m_0 is defined;[50] for the rotating disk electrode the mass transport coefficient, m_0, is given by eq 9b:[18,19]

$$m_0 = 0.62D^{2/3}\omega^{1/2}\nu^{-1/6} \tag{9b}$$

D is the diffusion coefficient of the substrate ($cm^2\ s^{-1}$), ω is the electrode angular rotation rate (s^{-1}) and ν is the kinematic viscosity constant (=0.01 $cm^2\ s^{-1}$ in water[51]).

Ideally, eq 9a would lead directly to an expression for S_0. However, in this case no analytical solution exists, and a numerical solution must be obtained. The voltammetric current is then given by eq 10, where n is the number of electrons transferred in the reaction and A is the electrode area (cm^2):

$$i = nFAm_0(S_B - S_0) \tag{10}$$

Possible Approximations to Provide an Analytical Solution for S_0. Under certain conditions (eq 11a), a Maclaurin series expansion (to the first-order term) can be used to derive a quadratic equation for S_0 from eq 9a:

$$S_0 = -\frac{p}{2} + \sqrt{\frac{p^2}{4} - q}$$

$$\text{for } \frac{K_m k_0^{max} a}{k_0^{max} + k_2 b} \cdot \frac{1}{S_0} \text{ and } \frac{K_m k_0^{min} a}{k_0^{min} + k_2 b} \cdot \frac{1}{S_0} \ll 1 \tag{11a}$$

$$p = aK_m - S_B + \frac{k_2\Gamma_{Total}}{m_0\beta d_0}\ln\left(\frac{k_0^{max} + k_2 b}{k_0^{min} + k_2 b}\right) \tag{11b}$$

$$q = \frac{k_2\Gamma_{Total}}{m_0\beta d_0}\left(\frac{k_0^{max} a K_m}{k_0^{max} + k_2 b} - \frac{k_0^{min} a K_m}{k_0^{min} + k_2 b}\right) - aK_m S_B \tag{11c}$$

Equation 11a was found to give a reasonable estimation of the current for parameter combinations which fulfill the stated boundary conditions. However, the boundary conditions are potential dependent and require knowledge of unknown parameters such as S_0 and k_0^{max}. In addition, eq 11a results in artifactual biphasic (staggered) waveshapes for $E_2 > E_1$ at low driving forces. Therefore, although the approximation may be useful for an initial evaluation of candidate parameters it cannot be applied with confidence to evaluation of an uncharacterized experimental data set.

Calculation of the limiting current ($E \to \infty$). As $E \to \infty$, $a \to 1$ and $b \to 0$, so that eq 9a can be simplified (eq 12a) to give an analytical solution for S_0 (eq 12b):

$$m_0(S_B - S_0) = \frac{k_2\Gamma_{Total}S_0}{S_0 + K_m} \tag{12a}$$

$$S_0 = \frac{1}{2}\left(-K_m + S_B - \frac{k_2\Gamma_{Total}}{m_0}\right) + \sqrt{\left(K_m - S_B + \frac{k_2\Gamma_{Total}}{m_0}\right)^2 + 4S_B K_m} \tag{12b}$$

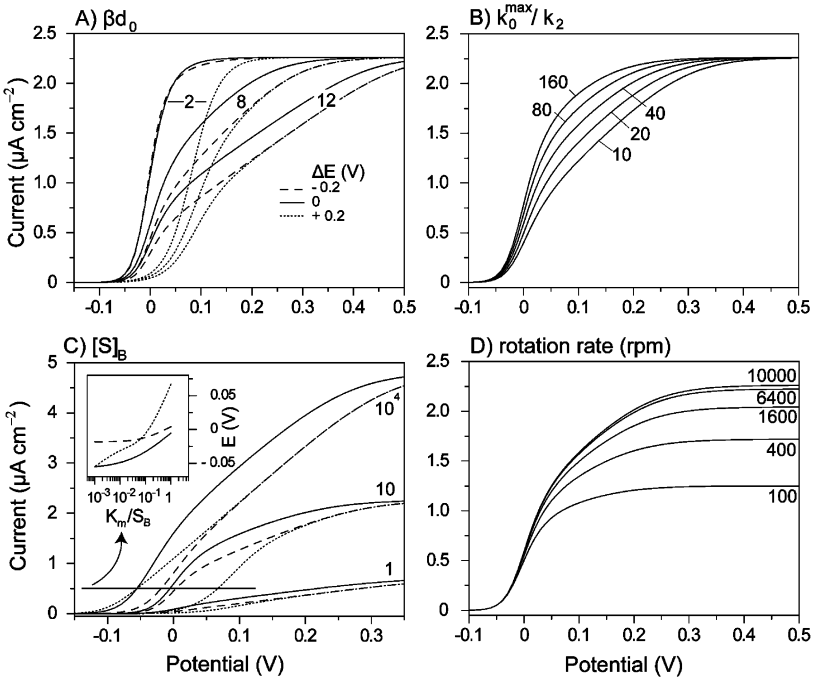

Figure 1. Typical voltammetric waveshapes generated using the model described. (A) Variation upon changing βd_0, for $\Delta E = -0.2$ V (dashed line), $\Delta E = 0$ V (solid line), and $\Delta E = +0.2$ V (dotted line). (B) Variation upon changing k_0^{max} (2500 to 40 000 s^{-1}), while k_2 is kept constant (250 s^{-1}). (C) How the voltammograms vary as the bulk substrate concentration varies. S_B is less than, equal to, and much greater than K_m (1 μM, 10 μM, and 10^4 μM (10 mM)). Results are presented for $\Delta E = -0.2$ V (dashed line), $\Delta E = 0$ V (solid line), and $\Delta E = +0.2$ V (dotted line). Inset: the "onset potential" is represented by the potential at which 0.5 μA is achieved, showing that the potential at which the voltammetric wave begins is lowest for $\Delta E = 0$ V, but that the relative onset potentials for $\Delta E = \pm 0.2$ V depend strongly on the substrate concentration. (D) Dependence on the electrode rotation rate (100 to 10 000 rpm: $\omega = 10.5-1050$ s^{-1}). Conditions unless otherwise specified: 30 °C, $D_{NADH} = 3.5$ cm^2 s^{-1}, $\nu = 0.01$ cm^2 s^{-1}, $E_{AV} = 0$ V, $\Delta E = 0$ V, $\Gamma_{Total} = 1 \times 10^{-13}$ mol cm^{-2}, $K_m = 10$ μM, $k_0^{max} = 10\,000$ s^{-1}, $k_2 = 250$ s^{-1}, $S_B = 10$ μM, $\beta d_0 = 8$, and $\omega = 1050$ s^{-1} (10 000 rpm).

Equation 12b applies to all experimental conditions, and provides i_{lim} by substitution into eq 10. Note that the limiting current as $E \rightarrow \infty$, i_{lim}, is independent of the model for interfacial electron transport which is applied, so that our equation is identical to those derived using simple Butler−Volmer (or Marcus) kinetics.[17]

When mass transport is not rate limiting ($m_0 \rightarrow \infty$), eq 12b shows that $S_0 \rightarrow S_B$. In this case, the overall rate of catalysis equals the rate of enzyme turnover, and i_{lim} can be derived from the right-hand side of eq 12a, and eq 10:

$$i_{lim} = nFAk_2\Gamma_{Total}\left(\frac{S_B}{S_B + K_m}\right) \qquad (13a)$$

Clearly, eq 13a is an electrochemical form of the Michaelis−Menten equation, and it can be used to define K_m (and k_2) if the appropriate experimental conditions can be applied [i_{lim} can be determined as $\omega \rightarrow \infty$ (see, for example,[16])].

When mass transport is completely limiting $S_0 \rightarrow 0$, so that the left-hand side of eq 9a can be used to define i_{lim}, in accordance with the Levich equation:[18]

$$i_{lim} = nFAm_0S_B \qquad (13b)$$

General Characteristics of the Model. Equation 9a demonstrates that the dependence of S_0 (and hence the catalytic current) on potential is a complicated function of a number of parameters. Therefore, it is difficult to describe concisely how the behavior of our model varies as any one of these parameters is changed. Figure 1 shows four sets of catalytic waveshapes, produced by typical sets of parameters, to give an overall picture.

The properties of the enzyme/electrode interface are described by βd_0 and k_0^{max}. Figure 1A shows that, as described previously by Léger and co-workers,[33] increasing βd_0 causes the voltammogram to deviate further from its ideal sigmoidal shape, so that the region in which current depends linearly on potential is extended. Figure 1B shows that this characteristic is modified by k_0^{max}/k_2, so that the voltammogram is most sigmoidal at small βd_0 and high k_0^{max}/k_2.

The properties of the enzyme are described by k_2, K_m, $E_{AV} = (E_1 + E_2)/2$ and $\Delta E = E_2 - E_1$. In Figure 1 $E_{AV} = 0$, and changing E_{AV} simply translates the voltammogram along the potential axis. The effect of changing k_2 is equivalent to the effect of changing k_0^{max}, since we have found that the waveshape is determined by the k_0^{max}/k_2 ratio (see below). This result is not apparent from eq 9a, but it is consistent with the behavior of Léger's model. Thus, the effect of changing k_2 is embodied in Figure 1B. Note that k_2 and k_0^{max} have different temperature dependencies (the catalytic reaction is expected to have a larger activation energy), so that higher temperatures reduce k_0^{max}/k_2 and produce more sloping voltammograms (see Figure 1B). Figures 1A and 1C show voltammograms with different ΔE values. In Figure 1A $S_B = K_m$ and the potential of the current onset depends strongly on ΔE. Interestingly, the current onset is at lowest potential when $\Delta E = 0$, and the curves for $\Delta E = +0.2$ V and -0.2 V merge before they merge with the curve for $\Delta E = 0$ V. This indicates that the onset potential is influenced by both E_1 and E_2, and that it shifts accordingly when one of them moves to high potential. Figure 1C shows how the voltammograms change as the bulk substrate concentration changes relative to K_m. As expected the current is largest when $S_B \gg K_m$, and the shapes of the voltammograms at a given S_B are strongly dependent on ΔE, particularly in the sigmoidal region of the wave. Note that substrate binding affects the "apparent" value of E_2, by affecting the O/I equilibrium, and

that the apparent values of E_1 and E_2 may be modulated, in practice, by binding to the I and R states at high substrate concentration (these extra bound states are not included in the current model). The inset to Figure 1C helps to illustrate how the current onset (represented by the potential at 0.5 μA cm^{-2}) varies with S_B, for the different ΔE values: in all cases $\Delta E = 0$ gives (close to) the lowest current onset potential.

Finally, Figure 1D shows how the voltammograms become less sigmoidal as m_0 increases (ω increases), and that the limiting current eventually becomes independent of ω as the voltammograms become mass transport independent.

Comparison with Heering's and Léger's models. Heering et al. used a reaction scheme analogous to that presented in Scheme 1B, and employed both mass transport according to the Levich equation, and the Michaelis−Menten equation.[17] However, only unique k_0 values were employed. As expected, the model described here gives results which are identical to those from Heering's equation if $\beta d_0 \rightarrow 0$ (the distribution becomes infinitely narrow and $k_0^{min} \rightarrow k_0^{max}$): eq 14, reproduced using our notation for comparison.

$$i = (nFA\Gamma_{Total}k_2) \div \left(1 + \frac{k_2}{k_0}b + \frac{2K_m a}{S_B}\left(1 - \frac{K_m m_0 a + k_2\Gamma_{Total}}{S_B m_0\left(1 + \frac{k_2}{k_0}b\right)} + \left(\left(1 - \frac{K_m m_0 a + k_2\Gamma_{Total}}{S_B m_0\left(1 + \frac{k_2}{k_0}b\right)}\right)^2 + \frac{4K_m a}{S_B\left(1 + \frac{k_2}{k_0}b\right)}\right)^{1/2}\right)^{-1}\right) \quad (14)$$

Heering's model produces only sigmoidal waveshapes (which vary with mass transport and substrate concentration), whereas the model described here produces waveshapes which do not reach i_{lim} until much higher potentials. The comparison is exemplified by the waveshapes presented in Figure 2.

Léger et al. used a different reaction scheme which did not take limitations from mass transport into account ($S_0 = S_B$, effectively $m_0 = \infty$).[33] Although Léger's scheme has been used[14,15] to investigate substrate−enzyme interactions via the dependence of E_1, E_2, and k_2 on S_B, we note that it is only a good approximation when $S_0 = S_B$. When mass transport cannot maintain S_0 equal to S_B, S_0 varies through the scan and effective values of E_1, E_2, and k_2 become potential dependent. This is most important when S_0 becomes comparable to (or lower than) K_m for at least part of the scan, and this is most likely to occur at low S_B and low rotation rate. Thus, our model predicts similar waveshapes to Léger's model when $m_0 \rightarrow \infty$ ($S_0 \rightarrow S_B$) and $K_m/S_B \rightarrow 0$, though, because of the different reaction schemes employed, they are never mathematically equivalent (Léger's model: eq 15; the appropriate limit of our model: eq 16).

$$i = \frac{nFA\Gamma_{Total}k_2}{a}\left(1 + \frac{1}{\beta d_0}\ln\frac{a + b\frac{k_2}{k_0^{max}}}{a + b\frac{k_2}{k_0^{max}}\exp(\beta d_0)}\right) \quad (15)$$

$$i = \frac{nFA\Gamma_{Total}k_2}{\beta d_0}\ln\left[\frac{k_0^{max} + k_2 b}{k_0^{max}\exp(-\beta d_0) + k_2 b}\right] \quad (16)$$

Numerical evaluation (using the same sets of parameters) shows that eqs 15 and 16 give similar results at higher potentials, but differ at lower potentials (Figure 3). They are very similar when

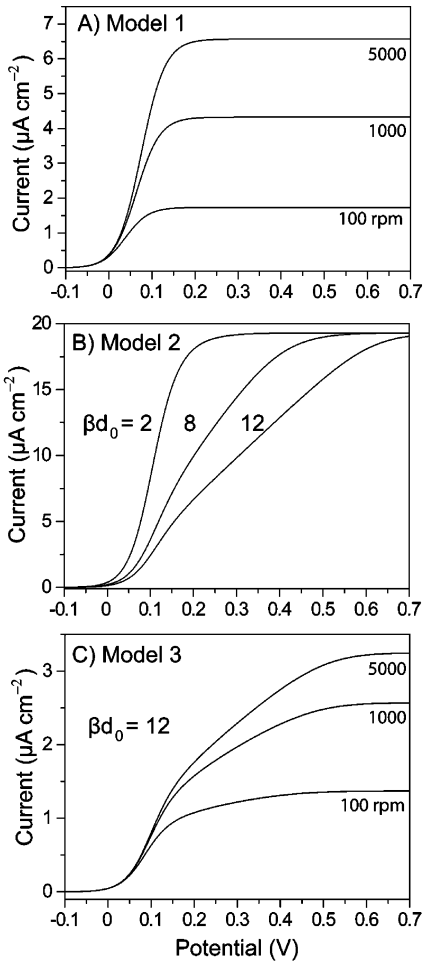

Figure 2. Representative predicted catalytic waveshapes from Heering's model (Model 1), Léger's model (Model 2), and the model described here (Model 3). Models 1 and 3 produce waveshapes which depend on mass transport to the electrode surface; models 2 and 3 account for a distribution in the interfacial electron-transfer rate constants. Conditions unless otherwise stated: 30 °C, $D_{NADH} = 3.5$ cm^2 s^{-1}, $\upsilon = 0.01$ cm^2 s^{-1}, $E_{AV} = 0$ V, $\Delta E = 0.2$ V, $\Gamma_{Total} = 1 \times 10^{-13}$ mol cm^{-2}, $K_m = 10$ μM, $S_B = 10$ μM, $k_2 = 1000$ s^{-1}, k_0 and $k_0^{max} = 10\,000$ s^{-1}.

$\Delta E = -0.2$ V, but differ very significantly when $\Delta E = +0.2$ V; the behavior when $\Delta E = 0$ is intermediate. Qualitatively, Léger's model resembles our model for small S_B at low driving force, then switches to the limiting curve for high S_B at high driving force. We suggest that the difference arises because K_m is defined separately from E_1, E_2, and k_2 in our model, whereas the effects of the enzyme−substrate interactions on E_1 and E_2 are included as equilibria in Léger's model. At high substrate concentration and high driving force our enzyme exists predominantly as OS, and k_2 strongly influences the catalytic rate. This situation is mechanistically equivalent to that which exists under Léger's model. At low driving force catalysis begins at lower potential, in our model, because the O/OS equilibrium facilitates the oxidation of I and R by removing O. Therefore, the "apparent" value of E_2 (from the point of view of Léger's model) is not the same as E_2 defined by our model. The difference is most noticeable when E_2 is high ($\Delta E > 0$) and exerting most influence (at lower overpotentials).

Results

Figure 4 shows an example dataset for catalytic NADH oxidation by subcomplex Iλ at 0.5 mM NADH and 1000 rpm

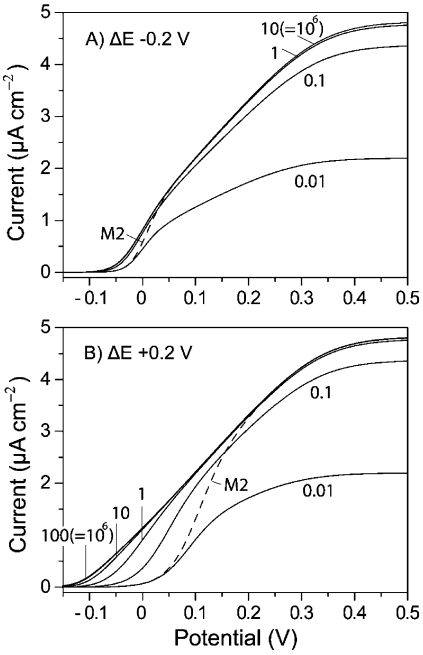

Figure 3. Comparison of the catalytic voltammograms predicted by Léger's model (M2) and the model described here at different substrate concentrations and high electrode rotation rate. As the substrate concentration (marked, in mM) of our model is increased the predicted voltammogram coalesces with that predicted by model 2 at high potential, but deviates significantly from it at low potential (see text). The difference is much more marked for $\Delta E = +0.2$ V (B) than for -0.2 V (A). Conditions: 30 °C, $D_{NADH} = 3.5$ cm^2 s^{-1}, $\upsilon = 0.01$ cm^2 s^{-1}, $E_{AV} = 0$ V, $\Gamma_{Total} = 1 \times 10^{-13}$ mol cm^{-2}, $k_0^{max} = 10\,000$ s^{-1}, $k_2 = 250$ s^{-1}, $K_m = 10$ μM, $S_B = 10$ μM, $\beta d_0 = 8$ and $\omega = 1050$s^{-1} (10 000 rpm).

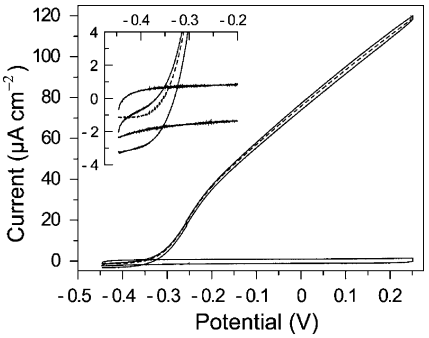

Figure 4. A typical voltammogram and its reference scan, demonstrating the validity of the data processing method. The forward and reverse scans were averaged then the reference scan was subtracted from the experimental data to obtain the final catalytic voltammogram (dashed line). Inset: the low potential reversal point showing the small systematic error which occurs in this region. Experimental conditions: 10 mV s^{-1}, 1000 rpm, 32 °C, 10 mM KCl + mixed buffer, pH 7.8, 0.5 mM NADH; reference scan recorded in the absence of subcomplex Iλ.

($\omega = 105$ s^{-1}) along with its reference scan, and demonstrates the validity of averaging the forward and reverse scans. Our data extraction procedure works well over most of the potential range, but gives a small discrepancy at low potentials (inset). This may be because the capacitance is altered slightly when the enzyme adsorbs, but it may also be due to small reductive currents which occur because product is retained at the electrode surface longer than expected. Figure 5 shows a set of voltammograms, derived from experiments, as shown in Figure 4, over a range of rotation rates and substrate concentrations. Scans recorded at 1000 rpm, but at different concentrations, are compared in Figure 5D. It is clear that Heering's model cannot describe the data from subcomplex Iλ, because the observed waveshapes are not sigmoidal (see Figure 2). Léger's model cannot explain all of the data presented either, because it contains no substrate or rotation rate dependency.

Fitting the Data at High Substrate Concentration and High Rotation Rate. A complete description using our model requires knowledge of a significant number of parameters. The temperature, bulk substrate concentration, and electrode rotation rate are set experimentally, but the diffusion coefficient to define the mass transport coefficient, βd_0, k_0^{max}, and ΓTotal to describe the enzyme/electrode interface, and E_{AV}, ΔE, k_2 and K_m to describe the enzyme, are not pre-defined. Table 1 presents information which is relevant to defining initial values and limits for each parameter. The data shown in Figure 5C have the highest substrate concentration (0.5 mM), and the highest rotation rate curve (2000 rpm) represents the limit of both parameters (further increase did not increase the current). At this limit the current is essentially independent of K_m and D_{NADH}, so the data can be fit without detailed knowledge of them. An initial screen for a total of 5250 combinations of ΔE, k_0^{max}, k_2, and βd_0 was defined as follows: $\Delta E = \pm 0.2$, ± 0.1, ± 0.05, and 0 V; $k_0^{max} = 5000$, 10 000, 20 000, 30 000, 40 000, and 50 000 s^{-1}; $k_2 = 100-2500$ s^{-1} in steps of 100; $\beta d_0 = 12-20$ in steps of 2. The aim was to explore the whole parameter space, avoiding local minima and finding all equally good combinations of parameters. Then, a voltammetric curve was calculated for each combination and compared to a set of 20 equally spaced experimental points. E_{AV} and Γ_{Total} were optimized for each combination using least-squares minimization; changes in E_{AV} translate the curve along the potential axis, and changes in Γ_{Total} affect the current magnitude. Finally, the quality of the fit was assessed for each combination of parameters using the least-squares-error (LSQ) value.

The results are presented in Figure 6. Figure 6A shows (for $\Delta E = 0$) how plotting the LSQ value against $\Gamma_{Total}k_2/\beta d_0$ allows an optimal value for this ratio to be determined. If $\beta d_0 < 14$ then an optimal fit is not achieved, but all the values of $\beta d_0 > 14$ gave essentially the same results. Figure 6B presents a similar approach for k_0^{max}/k_2. Therefore, for $\Delta E = 0$: $\beta d_0 \geq 14$, $\Gamma_{Total}k_2/\beta d_0 = 2.8 \times 10^{-11}$ mol cm^{-2} s^{-1}, and $k_0^{max}/k_2 = 19$. It was not possible to derive exact values for each individual parameter, as similar graphs show that no correlation exists. Similar analyses were carried out for each ΔE value. In all cases $\beta d_0 \geq 14$, and $\Gamma_{Total}k_2/\beta d_0$ did not vary significantly. Figure 6C shows that k_0^{max}/k_2 depends on ΔE in an approximately parabolic fashion around $\Delta E = 0$, and E_{AV} shows a small dependence on ΔE ($E_{AV} = -0.23$ to -0.26 V). Finally, Figure 6D shows overlays of the data and modeled curves generated for each ΔE using the best-hit parameters. It is obvious that an excellent fit is provided by each ΔE value, and so different values of ΔE cannot be distinguished at this stage. Note that a small discrepancy exists at low driving force. We believe this is because, although the NADH was purified before use, NAD^+ is formed during the course of the voltammogram (the scan presented in Figure 4 would generate $\sim$1.64 μM NAD^+) leading to a small reduction current at the most negative potentials.

As expected, the data obtained in this limiting case can be fit using Léger's model[33] also (using $\Delta E = 0$ V: $E_{AV} = -0.279$ V, $k_0^{max}/k_2 = 14.9$, and $i_{lim}/\beta d_0 = 0.16$ μA) to provide a fit which is of comparable quality to that described here. From our model, k_0^{max}/k_2 is 19, comparable to the value from Léger's model, and E_{AV} has shifted by $\sim$40 mV (-0.238 V) because in our model E_{AV} does not include thermodynamic contributions from substrate binding; $i_{lim}/\beta d_0$ is not defined.

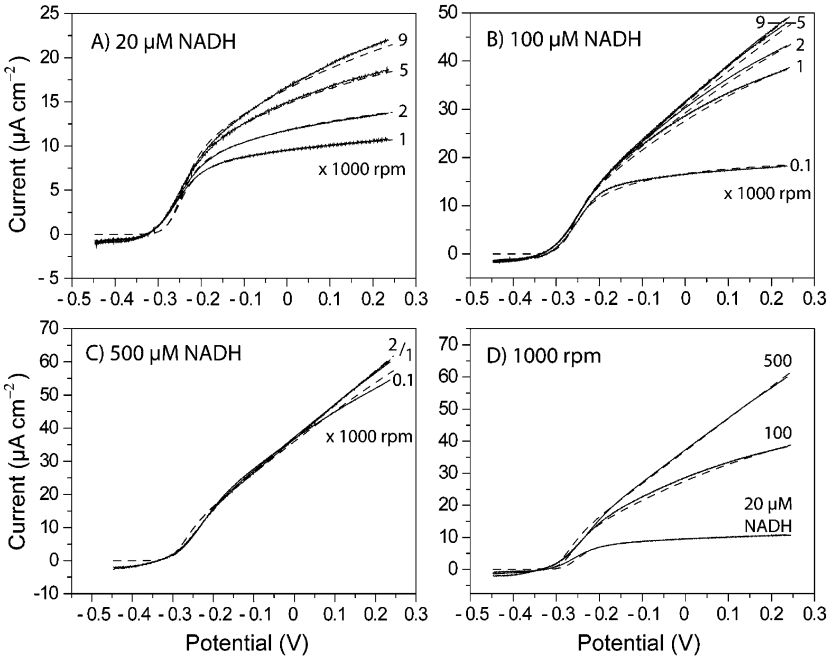

Figure 5. Electrocatalytic NADH oxidation by subcomplex Iλ coadsorbed with DDAB on a PGE electrode, over a range of rotation rates and NADH concentrations. Panels A−C show the results recorded at different NADH concentrations (20−500 μM) using different rotation rates (marked on figures, rpm). Panel D compares the three concentrations at 1000 rpm. Straight lines represent the measured data and dashed lines show the best overall fit (ΔE = 0 V, see text). Experimental conditions: 25 mV s^{-1}, 30 °C, 10 mM KCl + mixed buffer, pH 7.8.

TABLE 1: Previous Knowledge of the Variables Which Are Required to Fit the Experimental Data from Subcomplex Iλ

	expected value	justification	determined value
D (10^{-6} cm^2 s^{-1})	3.5−4.5	4.25 and 4.04 from Wilke-Chang[52] and Hayduk−Laudie[53] estimations (30 °C), 3.3 − measured value (23 °C)[54].	3.65−3.9
βd_0	<140	average β value for protein matrix is 1.4 Å^{-1} [20], approximate length of subcomplex 1λ is 100 Å[38]; largest distances may not contribute.	≥14 Γ_{Total}·$k_2/\beta d_0$ = 2.7−3.75 × 10^{-11} mol cm^{-2} s^{-1}
k_0^{max}(s^{-1})	no strong expectation	unique k_0 values: fastest value on PGE (azurin), 5000[47], >10^6 achieved using alkanethiol monolayers[55]; k_0^{max} for [NiFe]-hydrogenase, 30 000[33].	k_0^{max}/k_2 = 16−60
Γ_{Total} (mol cm^{-2})	<8.5 × 10^{-12}	estimated monolayer coverage on microscopically planar surface.	Γ_{Total}·$k_2/\beta d_0$ = 2.7−3.75 × 10^{-11} mol cm^{-2} s^{-1}
E_{av} (V)	−0.37 to −0.28 (pH 7.8)	values measured potentiometrically for FMN in complex I using redox mediators or NADH/NAD$^+$ [56].	−0.25
ΔE (V)	−0.2 to +0.2	−0.08 measured for complex I using redox mediators[56], but may not be relevant during catalysis.	−0.2 to +0.1
k_2 (s^{-1})	60−1000	turnover rate (NADH:ferricyanide) is ∼800. NADH:decylubiquinone (intact complex I) is ∼60[57]. However, may not be relevant to the voltammetric experiment due to different rate-limiting step.	k_0^{max}/k_2 = 16−60. Γ_{Total}·$k_2/\beta d_0$ = 2.7−3.75 × 10^{-11} mol cm^{-2} s^{-1}
K_m (μM)	no strong expectation	significant variation in reported values, values depend on identity of electron acceptor (see for example [58]).	33 ± 12.5

Fitting the complete set of substrate concentrations and rotation rates. The two ratios and the E_{AV} values defined above reduce the parameter space for fitting the complete data set. However, two additional parameters, D and K_m, must now be considered. Consequently, a low and high rotation rate voltammogram from each NADH concentration were each represented by 20 equally distributed data points as before, and used to calculate LSQ values with calculated curves. When comparing the values from curves with different final currents they were weighted by dividing by the sum of all current values to find the weighted least-squares-error (WLSQ). Calculations were carried out using the same set of ΔE values, for βd_0 from 12 to 20 in steps of 2, and for the same range of k_0^{max} as above. k_2 was set by the ratio of k_0^{max}/k_2 determined above, but allowed to vary by up to a factor of 2 from its predicted value. Initial values of Γ_{Total} (calculated from the ratio of $\Gamma_{Total}.k_2/\beta d_0$) and E_{AV} were set, but were then optimized separately for each substrate concentration to allow for small differences between the adsorbed films in the different experiments. Voltammograms were calculated for values of D from 2.5 to 4 × 10^{-6} cm^2 s^{-1} (steps of 0.25), and K_m of 1.25, 2.5, and from 5 to 50 μM in steps of 5 μM (note that some combinations were rapidly discarded as we noticed that large positive ΔE values required smaller D and K_m values, and vice versa). We confirmed that the optimal values found were not at the limit of variation of any parameter.

First, the average WLSQ value for the 100 best fits for each ΔE (out of 11 500 tested combinations) are presented in Figure 7A. ΔE = +0.2 V does not give such a good fit as ΔE from −0.2 to +0.1 V. In addition, Figure 7C shows that, for ΔE = +0.2 V, E_{AV} depends strongly on the experimental conditions (it should be invariant), and comparisons of calculated waveshapes with the experimental data showed significant deviation for the low-concentration dataset, and an incorrect dependence

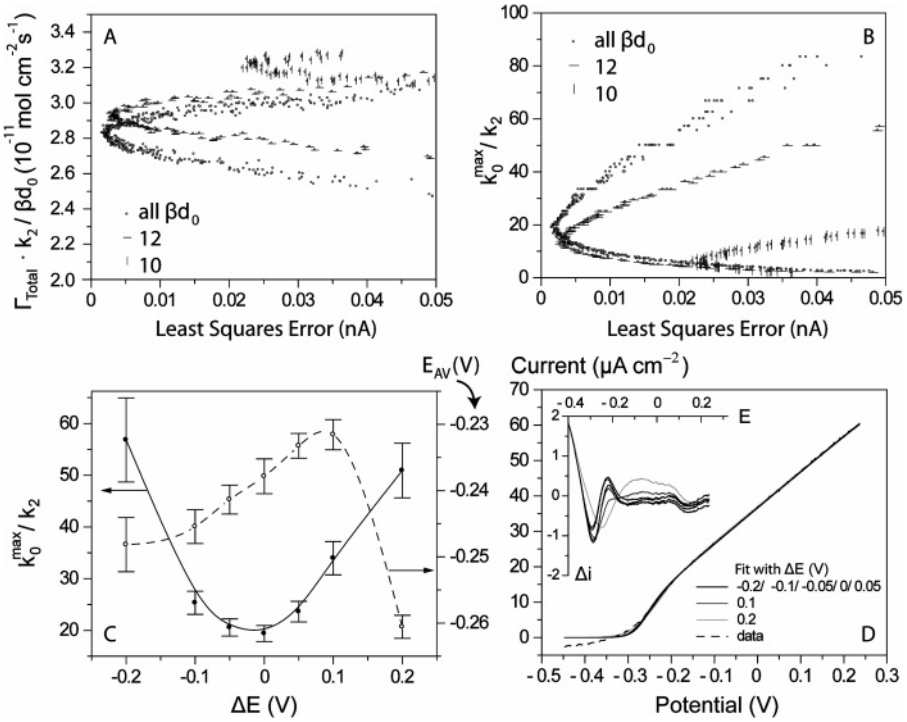

Figure 6. Results from fitting the high substrate concentration and high rotation rate data ([NADH] = 500 μM, 2000 rpm). (A) Variation in the LSQ value with $\Gamma_{Total} \times k_2/\beta d_0$, for $\Delta E = 0$ V. Only the low error region of the plot is shown, showing that the best fit is obtained with $\Gamma_{Total} \times k_2/\beta d_0 = 2.83 \times 10^{-11}$ mol cm^{-2} s^{-1}. Attempts to fit the data using $\beta d_0 = 10$ or 12 gave higher errors than fits using higher βd_0 values. (B) Variation in the LSQ value with k_0^{max}/k_2, for $\Delta E = 0$ V. Only the low error region of the plot is shown, and the best fit is obtained with $k_0^{max}/k_2 = 19.3$. Again, $\beta d_0 = 10$ or 12 gave higher errors than fits using higher βd_0 values. (C) Variation in the best fit values of k_0^{max}/k_2 (solid line, left-hand axis) and E_{AV} (dashed line, right-hand axis) as a function of the ΔE value used. (D) Overlay of the experimental data with fits using the best-fit values obtained at each ΔE value. Inset: the difference between data and fit is small at all potentials at which a substantial catalytic current is observed ($\Delta i < 1$ μA cm^{-2} for $E > -0.35$ V).

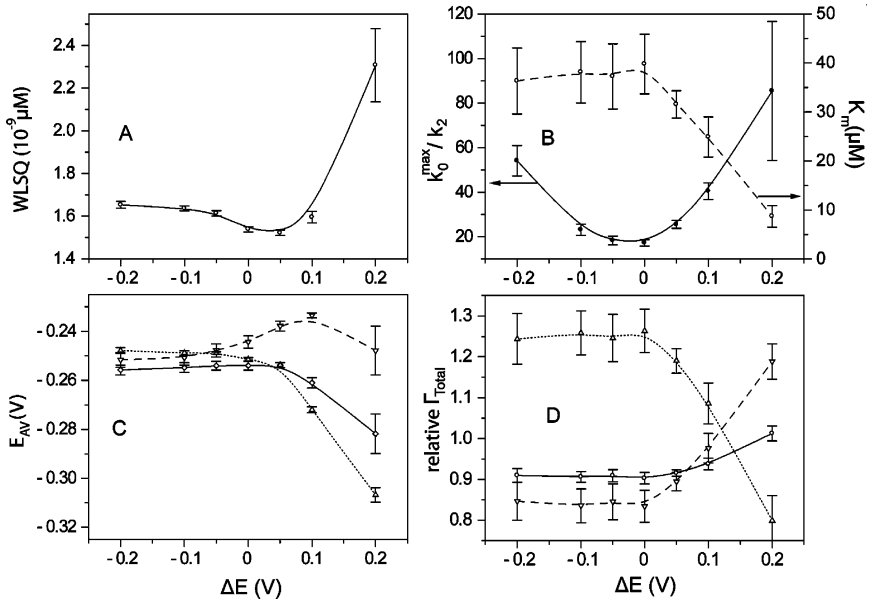

Figure 7. Results from fitting the complete dataset comprising different substrate concentrations and rotation rates. All results are presented for the best 100 fits (mean ± SD). (A) Variation in the WLSQ value with ΔE (see text). (B) Variation of the best-fit values of k_0^{max}/k_2 (solid line, left-hand axis) and K_m (dashed line, right-hand axis) as a function of the ΔE value used. (C) Variation of E_{AV} as a function of the ΔE value used; three values are reported for each ΔE, corresponding to each concentration of NADH (dotted line, 20 μM NADH; solid line, 100 μM NADH; dashed line, 500 μM NADH). (D) Variation of the relative Γ_{Total} values from each concentration of NADH as a function of the ΔE value used (dotted line, 20 μM NADH; solid line, 100 μM NADH; dashed line, 500 μM NADH).

of current on rotation rate (data not shown). Therefore, we do not consider $\Delta E = +0.2$ V further.

Figure 7B shows that k_0^{max}/k_2 varies with ΔE, and, although the ratio was allowed to vary again in the second round of fitting, very similar values to those obtained previously were found (except for $\Delta E = +0.2$ V). It also shows that, although K_m appears to depend slightly on the value of ΔE which is chosen, all the values are consistent with $K_m = 33 \pm 12.5$ μM ($\Delta E \neq +0.2$ V). In all cases $E_{AV} = -0.251 \pm 0.008$ V ($\Delta E \neq +0.2$ V). E_{AV} varies slightly between the three substrate concentra-

tions, and the fact that it varies least for $\Delta E \leq 0$ V provides some support for these values (Figure 7C). However, we note that E_{AV} may shift slightly in response to substrate binding to the fully or semi-reduced active site, which we have not allowed for in our current model. Conversely, in the ideal situation where every electrode preparation is identical, the relative Γ_{Total} values (relative $\Gamma_{Total} = 3\Gamma_{x\mu M}/\{\Gamma_{20\mu M} + \Gamma_{100\mu M} + \Gamma_{500\mu M}\}$) should all be 1; they agree most closely for $\Delta E = 0.1$ V (15% difference), but vary by 40% for $\Delta E \leq 0$ V (Figure 7D). However, as we cannot control or measure the electrode coverage, this observation cannot be used to support any of the ΔE values. D and $\Gamma_{Total}k_2/\beta d_0$ follow similar trends to K_m. $\Gamma_{Total}k_2/\beta d_0$ is constant at 3.50 ($\pm$0.24) $\times$ 10^{-11} mol cm^{-2} s^{-1} for $\Delta E \leq 0$ V, then decreases to 2.85 ($\pm$0.14) $\times$ 10^{-11} mol cm^{-2} s^{-1} for $\Delta E = 0.1$ V. D is constant at 3.89 ($\pm$0.125) $\times$ 10^{-6} cm^2 s^{-1} for $\Delta E \leq 0$ V, then decreases to 3.66 ($\pm$0.119) $\times$ 10^{-6} cm^2 s^{-1} for $\Delta E = 0.1$ V. Finally, for $\Delta E \leq -0.05$ V and $\Delta E = +0.2$ V $\beta d_0 \geq 14$ gave the best values, whereas $-0.05 \leq \Delta E \leq 0.1$ V required $\beta d_0 \geq 16$. Spot tests using higher βd_0 values (up to 50) showed no differences in the shape of the curves. Finally, note that the determined ratios described above imply realistic values of the individual parameters. For example, for $k_2 = 800$ s^{-1}, possible k_0^{max} values are 16 000 to 48 000 s^{-1}, and, with $\Gamma_{Total} = 1 \times 10^{-12}$ mol cm^{-2}, βd_0 is 24.

Figure 5 includes the fit to the data calculated from the single set of best-fit parameters obtained using $\Delta E = 0$ V. The fit is excellent over the whole range of voltammograms. However, all ΔE values, except 0.2 V, give fits which are of comparable quality, precluding determination of ΔE by this method.

Discussion

The catalytic voltammetry from an adsorbed enzyme is the result of a complex interplay of mass transport, enzyme turnover, and electron transfer, and all of these need to be controlled (and understood) before catalytic cyclic voltammograms can be exploited to give mechanistic information. The model presented here has been tested, using electrocatalytic NADH oxidation by subcomplex Iλ, under conditions in which each of the three regimes are rate limiting and demonstrated to be accurate in all cases. The rate of substrate supply has been varied by altering the electrode rotation rate, high and low substrate concentrations have been used to confer fast and slow rates of turnover according to the Michaelis−Menten equation, and different electrode potentials vary the rate of interfacial electron transfer. Therefore, though modifications of the model may be necessary to allow for an enzyme which does not obey the Michaelis−Menten equation, our model is relevant to the general case of an adsorbed electroactive enzyme.

Comparison of modeled voltammograms with experimental data allows identification of the rate-limiting step. When mass transport is fast and substrate concentration high the interfacial electron-transfer kinetics exert their most rate-limiting effect, as observed in Figure 5C for subcomplex Iλ. The "sloping" voltammogram, and our ability to model it as described, provides strong support for a dispersion of interfacial rate constants as proposed by Léger and co-workers.[33] Interestingly, although subcomplex Iλ is a very large molecule suggesting that βd_0 should be correspondingly large (Table 1), the data can be modeled using $\beta d_0 > 16$. This is because our experimental potential range does not extend far enough to allow larger values to be distinguished. In addition, very large electron transfer distances give very small rate constants and thus do not contribute significantly to the overall rate. Our data depend on the substrate concentration also, and thus allow determination of a K_m value, approximately 33 μM NADH (30 °C, pH 7.8). Our value is consistent with the range of values reported in the literature (see, for example, ref 58), but, as expected, K_m depends on which electron acceptor is used (ferricyanide, hexaamine ruthenium III, decylubiquinone, O_2) because k_2 varies, and on which definition of k_2 is used (whether k_2 applies to the complete reaction or only the catalytic half-reaction). Our voltammograms also depend on the rate of substrate mass transport, described by the diffusion coefficient, D. The value determined, 3.65−3.9 $\times$ 10^{-6} cm^2 s^{-1} is between the reported experimental value of 3.3 $\times$ 10^{-6} cm^2 s^{-1} [54] and the estimated values of approximately 4.25 $\times$ 10^{-6} cm^2 s^{-1} [52,53] (see Table 1). Finally, variation of the electrode potential defines E_{AV} accurately, but, perhaps surprisingly, does not discriminate between different values for ΔE. E_{AV} is the only parameter which does not lie within its predicted range (see Table 1), since it is considerably higher than the two-electron potential for the FMN cofactor in complex I.[56] We propose two possible explanations, which we aim to test in future experiments: (i) NADH is always present in our experiment, and EPR studies revealed a shift in the observed potential to −0.286 V when the redox titrations were carried out using NADH/NAD^+, instead of a mixture of redox mediator dyes.[56] However, relative stabilization of the reduced state is most likely to result from NAD^+ binding, and in our experiment, this can result only from reoxidation of $FMNH^-$/$FMNH_2$ before NAD^+ dissociates. Although such a mechanism has been proposed previously to operate in some conditions[59] it would have marked consequences for proton translocation by complex I since it implies that energy is retained by the FMN/NAD^+ site after the electrons have transferred, either reducing the efficiency of energy transduction or requiring a mechanism for energy transduction coupled to NAD^+ release. (ii) E_{AV} is reporting on a potential-dependent rate limiting step in enzyme turnover, which is not explicitly included in our current model. In particular, we note that four of the iron−sulfur clusters in complex I are reported to have reduction potentials around −0.25 V,[60] consistent with our determined value for E_{AV}. Therefore, it is possible that catalysis is impeded when the chain of clusters is reduced under steady-state conditions, and that catalysis "switches on" only when the chain is emptied and electron flow from the reduced flavin to the electrode is kinetically unimpeded.

The remaining parameters in our model have not been determined, but ratios and limits have been defined and form a parameter space. Indeed, our fitting procedure was specifically intended to explore the whole (reasonable) parameter space and avoid local minima that may lead, misleadingly, to a unique solution. In the future, further data may provide the opportunity to derive exact values for some, or all, of these parameters. For example, an independent value for Γ_{Total} would significantly reduce the parameter space; therefore, we aim to improve our electrode coverage to visualize noncatalytic voltammetric waves. Complex I and subcomplex Iλ will catalyze the oxidation of NADPH[61] but with different kinetic parameters to the oxidation of NADH, thus affecting enzyme turnover without altering the other physical parameters of the voltammetric experiment. Similar comparisons may be made by carrying out experiments in D_2O, at different temperatures or pH values, or in the presence of inhibitors, which act at the NADH binding site.[58] Experiments to study the reverse reaction, NAD^+ reduction, are also viable,[40] and may place further constraints on the mechanism.

In conclusion, the model described here provides an important advance in understanding and deconvoluting the behavior of enzymes adsorbed on electrode surfaces, and it allows the

extraction of mechanistically important information, even when the observed behavior is influenced by nonideal electron-transfer kinetics.

Acknowledgment. We thank Dr. Richard J. Shannon for expert advice on the preparation of subcomplex Iλ. This work was supported by The Medical Research Council.

References and Notes

(1) Armstrong, F. A. *Curr. Opin. Chem. Biol.* **2005**, *9*, 110−117.
(2) Léger, C.; Elliott, S. J.; Hoke, K. R.; Jeuken, L. J. C.; Jones, A. K.; Armstrong, F. A. *Biochemistry* **2003**, *42*, 8653−8662.
(3) Armstrong, F. A.; Wilson, G. S. *Electrochim. Acta* **2000**, *45*, 2623−2645.
(4) Armstrong, F. A.; Heering, H. A.; Hirst, J. *Chem. Soc. Rev.* **1997**, *26*, 169−179.
(5) Butt, J. N.; Sucheta, A.; Armstrong, F. A.; Breton, J.; Thomson, A. J.; Hatchikian, E. C. *J. Am. Chem. Soc.* **1993**, *115*, 1413−1421.
(6) Duff, J. L. C.; Breton, J. L. J.; Butt, J. N.; Armstrong, F. A.; Thomson, A. J. *J. Am. Chem. Soc.* **1996**, *118*, 8593−8603.
(7) Butt, J. N.; Fawcett, S. E. J.; Breton, J.; Thomson, A. J.; Armstrong, F. A. *J. Am. Chem. Soc.* **1997**, *119*, 9729−9737.
(8) Hirst, J.; Duff, J. L. C.; Jameson, G. N. L.; Kemper, M. A.; Burgess, B. K.; Armstrong, F. A. *J. Am. Chem. Soc.* **1998**, *120*, 7085−7094.
(9) Camba, R.; Armstrong, F. A. *Biochemistry* **2000**, *39*, 10587−10598.
(10) Hudson, J. M.; Heffron, K.; Kotlyar, V.; Sher, Y.; Maklashina, E.; Cecchini, G.; Armstrong, F. A. *J. Am. Chem. Soc.* **2005**, *127*, 6977−6989.
(11) Heering, H. A.; Wiertz, F. G. M.; Dekker, C.; de Vries, S. *J. Am. Chem. Soc.* **2004**, *126*, 11103−11112.
(12) Elliott, S. J.; Hoke, K. R.; Heffron, K.; Palak, M.; Rothery, R. A.; Weiner, J. H.; Armstrong, F. A. *Biochemistry* **2004**, *43*, 799−807.
(13) Gwyer, J. D.; Richardson, D. J.; Butt, J. N. *Biochemistry* **2004**, *43*, 15086−15094.
(14) Léger, C.; Jones, A. K.; Roseboom, W.; Albracht, S. P. J.; Armstrong, F. A. *Biochemistry* **2002**, *41*, 15736−15746.
(15) Hoke, K. R.; Cobb, N.; Armstrong, F. A.; Hille, R. *Biochemistry* **2004**, *43*, 1667−1674.
(16) Sucheta, A.; Cammack, R.; Weiner, J.; Armstrong, F. A. *Biochemistry* **1993**, *32*, 5455−5465.
(17) Heering, H. A.; Hirst, J.; Armstrong, F. A. *J. Phys. Chem. B* **1998**, *102*, 6889−6902.
(18) Levich, V. G. *Physicochemical Hydrodynamics*; Prentice Hall: New Jersey, 1962.
(19) Bard, A. J.; Faulkner, L. R. *Electrochemical Methods, 2nd ed.*; Wiley: New York, 2001.
(20) Page, C. C.; Moser, C. C.; Chen, X.; Dutton, P. L. *Nature* **1999**, *402*, 47−52.
(21) Marcus, R. A. *Angew. Chem., Int. Ed. Engl.* **1993**, *32*, 1111−1121.
(22) Chidsey, C. E. D. *Science* **1991**, *251*, 919−922.
(23) Blankespoor, R.; Limoges, B.; Schöllhorn, B.; Syssa-Magalé, J.-L.; Yazidi, D. *Langmuir* **2005**, *21*, 3362−3375.
(24) Ataka, K.; Heberle, J. *J. Am. Chem. Soc.* **2004**, *126*, 9445−9457.
(25) Armstrong, F. A.; Barlow, N. L.; Burn, P. L.; Hoke, K. R.; Jeuken, L. J. C.; Shenton, C.; Webster, G. R. *Chem. Commun.* **2004**, 316−317.
(26) Zhang, J.; Welinder, A. C.; Hansen, A. G.; Christensen, H. E. M.; Ulstrup, J. *J. Phys. Chem. B* **2003**, *107*, 12480−12484.
(27) El Kasmi, A.; Wallace, J. M.; Bowden, E. F.; Binet, S. M.; Linderman, R. J. *J. Am. Chem. Soc.* **1998**, *120*, 225−226.
(28) Jeuken, L. J. C. *Biochim. Biophys. Acta* **2003**, *1604*, 67−76.
(29) Chen, P.; Fryling, M. A.; McCreery, R. L. *Anal. Chem.* **1995**, *67*, 3115−3122.
(30) McDermott, M. T.; McDermott, C. A.; McCreery, R. L. *Anal. Chem.* **1993**, *65*, 937−944.
(31) Cabaniss, G. E.; Diamantis, A. A.; Murphy, W. R.; Linton, R. W.; Meyer, T. J. *J. Am. Chem. Soc.* **1985**, *107*, 1845−1853.
(32) Randin, J.-P.; Yeager, E. *J. Electroanal. Chem.* **1975**, *58*, 313−322.
(33) Léger, C.; Jones, A. K.; Albracht, S. P. J.; Armstrong, F. A. *J. Phys. Chem. B* **2002**, *106*, 13058−13063.
(34) Hirst, J. *Biochem. Soc. Trans.* **2005**, 525−529.
(35) Walker, J. E. *Q. Rev. Biophys.* **1992**, *25*, 253−324.
(36) Fearnley, I. M.; Carroll, J.; Shannon, R. J.; Runswick, M. J.; Walker, J. E.; Hirst, J. *J. Biol. Chem.* **2001**, *276*, 38345−38348.
(37) Finel, M.; Majander, A. S.; Tyynelä, J.; De Jong, A. M. P.; Albracht, S. P. J.; Wikström, M. *Eur. J. Biochem.* **1994**, *226*, 237−242.
(38) Hinchliffe, P.; Sazanov, L. A. *Science* **2005**, *309*, 771−774.
(39) Hirst, J.; Carroll, J.; Fearnley, I. M.; Shannon, R. J.; Walker, J. E. *Biochim. Biophys. Acta* **2003**, *1604*, 135−150.
(40) Zu, Y.; Shannon, R. J.; Hirst, J. *J. Am. Chem. Soc.* **2003**, *125*, 6020−6021.
(41) Léger, C.; Dementin, S.; Bertrand, P.; Rousset, M.; Guigliarelli, B. *J. Am. Chem. Soc.* **2004**, *126*, 12162−12172.
(42) Orr, G. A.; Blanchard, J. S. *Anal. Biochem.* **1984**, *142*, 232−234.
(43) Lu, Z.; Huang, Q.; Rusling, J. F. *J. Electroanal. Chem.* **1997**, *423*, 59−66.
(44) Nassar, A.-E. F.; Zhang, Z.; Hu, N.; Rusling, J. F.; Kumosinski, T. F. *J. Phys. Chem. B* **1997**, *101*, 2224−2231.
(45) Schweiss, R.; Werner, C.; Knoll, W. *J. Electroanal. Chem.* **2003**, *540*, 145−151.
(46) White, H. S.; Peterson, J. D.; Cui, Q.; Stevenson, K. J. *J. Phys. Chem. B* **1998**, *102*, 2930−2934.
(47) Hirst, J.; Armstrong, F. A. *Anal. Chem.* **1998**, *70*, 5062−5071.
(48) Avraam, R.; Kotlyar, A. B. *Biochemistry (Moscow)* **1991**, *56*, 1181−1189.
(49) Segel, I. H. *Enzyme Kinetics: Behavior and Analysis of Rapid Equilibrium and Steady-State Enzyme Systems*; Wiley: New York, 1975.
(50) Armstrong, F. A.; Bond, A. M.; Büchi, F. N.; Hamnett, A.; Hill, H. A. O.; Lannon, A. M.; Lettington, O. C.; Zoski, C. G. *Analyst* **1993**, *118*, 973−978.
(51) Weast, R. C. (Ed.) *Handbook of Chemistry and Physics, 61st ed.*; CRC Press: Boca Raton, FL, 1981.
(52) Wilke, C. R.; Chang, P. *Am. Inst. Chem. Eng. J.* **1955**, *1*, 264−270.
(53) Hayduk, W.; Laudie, H. *Am. Inst. Chem. Eng. J.* **1974**, *20*, 611−615.
(54) Rostovtseva, T. K.; Komarov, A.; Bezrukov, S. M.; Colombini, M. *Biophys. J.* **2002**, *82*, 193−205.
(55) Smalley, J. F.; Feldberg, S. W.; Chidsey, C. E. D.; Linford, M. R.; Newton, M. D.; Liu, Y.-P. *J. Phys. Chem.* **1995**, *99*, 13141−13149.
(56) Sled, V. D.; Rudnitzky, N. I.; Hatefi, Y.; Ohnishi, T. *Biochemistry* **1994**, *33*, 10069−10075.
(57) Sharpley, M. S.; Shannon, R. J.; Draghi, F.; Hirst, J. *Biochemistry* **2006**, *45*, in press.
(58) Zharova, T. V.; Vinogradov, A. D. *Biochim. Biophys. Acta* **1997**, *1320*, 256−264.
(59) Gavrikova, E. V.; Grivennikova, V. G.; Sled, V. D.; Ohnishi, T.; Vinogradov, A. D. *Biochim. Biophys. Acta* **1995**, *1230*, 23−30.
(60) Ohnishi, T. *Biochim. Biophys. Acta* **1998**, *1364*, 186−206.
(61) Hatefi, Y.; Hanstein, W. G. *Biochemistry* **1973**, *12*, 3515−3522.